

# Effective Image Representations for Tree Pollen Recognition

Alicja Wieczorkowska<sup>1</sup>[0000–0003–2033–6372], Elżbieta Kubera<sup>2</sup>[0000–0003–3447–9569] (✉), Agnieszka Kubik-Komar<sup>2</sup>[0000–0002–4258–0133], Krystyna Piotrowska-Weryszko<sup>3</sup>[0000–0003–3827–3218], and Agata Konarska<sup>3</sup>[0000–0003–2174–7608]

<sup>1</sup> Department of Multimedia, Polish-Japanese Academy of Information Technology,  
Koszykowa 86, Warsaw, Poland [alicja@poljap.edu.pl](mailto:alicja@poljap.edu.pl)

<sup>2</sup> Department of Applied Mathematics and Computer Science, University of Life Sciences in Lublin, Akademicka 13, Lublin, Poland  
[{elzbieta.kubera,agnieszka.kubik}@up.lublin.pl](mailto:{elzbieta.kubera,agnieszka.kubik}@up.lublin.pl)

<sup>3</sup> Department of Botany and Plant Physiology, University of Life Sciences in Lublin,  
Akademicka 13, Lublin, Poland  
[{krystyna.piotrowska,agata.konarska}@up.lublin.pl](mailto:{krystyna.piotrowska,agata.konarska}@up.lublin.pl)

**Abstract.** More than one-third of the world population suffers from allergy symptoms, thus pollen monitoring is performed worldwide, to provide data on pollen seasons for people with allergies. To this end, Hirst traps that catch the airborne pollen grains and other particles are often used, and then specialists count the pollen grains of each taxon under microscope. This is a tedious task, so we would like to automate recognition and counting using deep learning-based object detectors. In this work, we investigate how changing the color representation affects pollen grain detection in images. Five different representations were examined: RGB, AvgRGB, STRESS, CMYK, and Magenta, which we believe may be particularly useful, as pollen is dyed pink with fuchsin to improve visibility under a microscope. The average precision results for the investigated detectors are above 98% when both training and test data come from the same camera. However, precision decreases when the test data come from a different camera. We observed that only the conversion of images to Magenta allows for high pollen detection precision in images from a different camera than the one used to capture the training samples.

**Keywords:** image processing · image recognition · pollen monitoring

## 1 Introduction

Many people suffer from allergies nowadays; allergies are the sixth leading cause of chronic disease in the U.S. [18]. Inhalant allergies are particularly troublesome, because while we can avoid allergenic foods or substances in the case of food or skin allergies, it might be very difficult to avoid allergenic pollen when living in an area with allergenic plants. Symptoms of pollen allergy are disrupting

daily life, and the healthcare costs of pollen allergies have been exponentially increasing since the 1970s, estimated at 130 billion euros per year in Europe [19]. Collecting and analyzing data on pollen concentration in the air leads to increased availability of up-to-date information on the threat posed by high concentrations of allergenic pollen, the prediction of peak allergy periods, and consequently to a better mechanism for allergy control and prevention.

A volumetric spore trap based on Hirst's design is the most commonly used method of pollen monitoring [12]. A drum with an adhesive-coated transparent plastic band rotates slowly, and particles in the air stick to the tape. The air flow aspiration is at the rate corresponding to human breathing. The material from the trap is collected usually once a week, sliced into segments corresponding to days, and the pollen grains are recognized and counted under the microscope. The total grain number is then recalculated per cubic meter of air.

The recognition and counting of pollen grains of different taxa is performed by a palynologist (pollen specialist). This process is very labor-intensive, as during the pollen season trees can produce even 12,000 pollen grains in the cubic meter of air per day. It can take a palynologist several hours at the microscope to recognize and count pollen grains from one slide from the pollen trap, corresponding to one day of monitoring. Therefore, palynologists are interested in getting help in this process, and researchers working in the information technology area are looking for solutions to automate pollen monitoring [15, 7]; allergy sufferers are also interested in easy access to up-to-date monitoring results.

The increase of the number of monitoring stations would allow more precise monitoring of the aerobiological conditions, as pollen seasons vary significantly in different regions, and even the same location can show significant differences in various years. The automation of pollen counting would shorten the time of palynologists' work, and the results could be available on an ongoing basis.

### 1.1 Main Contributions

The final goal of our work is to automate the pollen monitoring process, to save the palynologists' time, and provide faster access to the monitoring outcomes, which is important for palynologists and allergy sufferers.

To facilitate ground truth labeling, we used reference material, with only one taxon represented in one image. Slides with pollen are stained with basic fuchsin, i.e., magenta dye. The level of color intensity depends on the amount of the fuchsin applied and the duration of the material exposition to it, as well as the camera properties, but does not depend on the taxon.

In this paper, we investigate whether changing the color representation influences the quality of taxon recognition. We believe that RGB (Red Green Blue) image representation may not be optimal for working with pinkish images. Since the shape (not the color) is the most important indicator to classify objects into particular taxa, we investigated other representations: CMYK (Cyan Magenta Yellow Black), Magenta (only one component from CMY (Cyan Magenta Yellow), which can be easily calculated from RGB), and Grayscale, calculated using two different approaches.

We trained the detectors with images coming from a single camera, and the performance was tested on two sets of images: 1) images different from the training and validation sets, captured with the same camera, and 2) images from a different camera. Next, we investigated whether there are significant differences in the detection results between the different color representations, and also between the two cameras, for the models yielding the highest detection precision. The obtained results indicate that the deep learning based detectors work best when Magenta representation is used instead of RGB. Therefore, proper image representation improves the detection results.

## 2 Related Work

The existing real-time automated pollen monitoring systems are based on various approaches, different than the Hirst's method, like DNA metabarcoding [4], deep learning and multispectral imaging flow cytometry [8], and the use of the combination of fluorescein and propidium iodide, with manual data labeling [2]. The results obtained from the automated systems often differ from the manually elaborated data [22]. Crowdsourcing is also used in the online project [17] that collates information from various reference collections, and allows the use of crowdsourcing in the pollen identification tasks via a dedicated online platform.

The automation of pollen identification in images from a microscope has long been a research topic [9, 5]. In such studies, the occurrence of pollen from each taxon is counted. Recently, deep learning has been extensively used for this purpose, including convolutional neural networks [26, 3]; approaches based on semi-automatic labeling, combining human expertise and machine learning, are also used [22]. However, it is hard to compare the outcomes of these works, as various data sets are used in these experiments.

YOLO (You Only Look Once) [1] system for object detection in images, has already been applied in automated pollen grain detection, using a device similar to the Hirst's trap [5], yielding good results even for 16 taxa. In [21], convolutional neural networks were used for pollen analysis, trained using data representing 122,000 pollen grains, from 347 flowers of 83 species of 17 families, and validated on 370 samples, representing pollen from pollen baskets of bumblebees' legs.

## 3 Materials and Methods

In North, Central, and Eastern Europe birch produces the most allergenic pollen. Therefore, we decided to investigate the automatic recognition of pollen grains for the birch family, *Betulaceae*, namely *Alnus*, *Betula*, and *Corylus*. These taxa have strong allergenic properties, their pollen grains have similar structural features, occur in high concentrations (especially *Betula* and *Alnus*), and can be recorded at the same time. Additionally, microscopy images acquired from Hirst-type traps usually contain grains of various species (as well as fungal spores, dust, etc). We chose YOLO for object detection, as it proved successful in similar studies [14, 15], and our goal was to investigate image representations, rather than

image detection models. Object detectors find regions in the image that correspond to particular pollen grains, and classify them into target classes (taxa).

### 3.1 Biological Material

The biological material we use represents the images of tree pollen. Our target classes are three taxa: *Betula*, *Corylus*, and *Alnus*. The species covered in this work are *Alnus glutinosa* (L.) Gaertn., *Corylus avellana* L., and *Betula pendula* Roth. *Betula* pollen is a major cause of allergic symptoms in the spring. Moreover, cross-reaction between the pollen *Betula*, *Corylus*, and *Alnus* prolongs the duration of allergy symptoms in many patients, as *Betula* pollen allergy sufferers often also react allergic to the pollen of the other two taxa. Although the *Alnus* and *Corylus* pollen grains appear in the air at the same time, and birch produces pollen later, there is still a partial overlap of pollen seasons, thus the pollen grains of all three investigated taxa can be found in the traps concurrently. Moreover, the pollen grains of these taxa look similar, especially *Betula* and *Corylus*. Therefore, correct identification of each taxon may be difficult, but we know that the pollen grains of *Betula* are of the smallest size, *Betula* and *Corylus* usually have three pores, and *Alnus* pollen has more pores. This can be used to guide proper identification of the pollen grains of these taxa, although some features may not be visible in the image, depending on the grain's position.

To avoid tedious manual ground-truth labeling of data from pollen monitoring, which may include dirt, spores, and other taxa, reference material for the investigated species was used. Examples of microscopy images of the pollen grains of *Alnus*, *Betula*, and *Corylus* are shown in Fig. 1. Glycerinated gelatine with basic fuchsin was used to stain the pollen grains pink. The degree of pollen coloring is independent of taxa. The camera applied to take photographs can also change coloring, see Fig. 1 b, where the background is colored pink.

### 3.2 Image data

A light microscope Eclipse E400 by Nikon was applied in this work, with 400x (standard magnification) or 600x magnification, thus the target objects (pollen grain) were captured at various scales. We used two cameras for acquiring image data from the microscope: Olympus DP 23 microscope camera with 400x magnification, in most cases, and HDCE-x5 microscope camera with 600x magnification, to capture morphological details of pollen grains. In manual pollen counting, 400x magnification is used, because lower magnification requires less work of the specialists, as fewer segments of the acquired material are analyzed.

### 3.3 Object Detection in Images

The similarity of pollen grains from different classes (especially *Betula* and *Corylus*) introduces inter-class similarities, and 2-dimensional representation of grains introduces intra-class differences, as grains from the same class may then look different. We applied deep learning based approach to deal with these difficulties.

In automated object detection in images, the position of an object of interest has to be found, and the object is then classified into predefined classes. A bounding box is used to mark the position and size of the object. In two-stage detection, the first step consists in determining regions of interest (RoI), and classification is performed on each RoI in the second step. In one-stage detection, bounding box is found and the object is classified in one step, for each object.

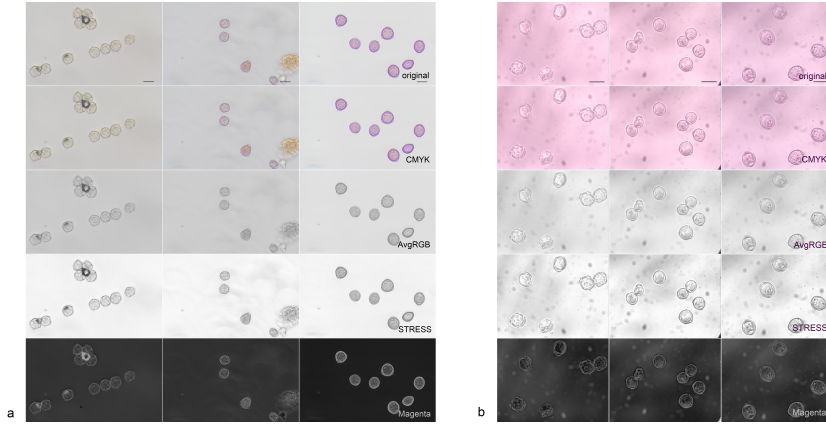


**Fig. 1.** Exemplary images taken with: a) Olympus DP 23 microscope camera, b) HDCE-x5 camera, shown in original RGB version and converted to the selected representations (left column: *Alnus*, middle column: *Betula*, right column: *Corylus*). The scale bar in the lower right corner of each image in the top row is equal to  $20 \mu\text{m}$ .

YOLO [24] is a one-stage detector, in which the input image is divided into  $N \times N$  grid, and then the bounding box is found within each cell of the grid. Faster Region-based Convolutional Neural Networks (Faster R-CNN) [25] is a 2-stage detector. A simplified approach, DETection TRAnsformers (DETR) [6], uses a transformer encoder-decoder architecture.

We decided to use YOLO, already applied in pollen detection [15]. We used models pre-trained on COCO database [16], and then fine-tuned the detector on our data, following the transfer-learning approach.

### 3.4 Image Representations

Since all images are colored using basic fuchsia, and the shape (not the color) is the main feature that indicates the taxon, we decided to apply four other image representations, in addition to the original RGB representation:

- CMYK;
- Magenta (single channel taken from CMYK);
- AvgRGB - grayscale, calculated as an average of RGB channels;

- STRESS - grayscale, calculated using the approach described in [13].

In particular, Magenta seems to be suitable for images with the pink coloration of pollen grains, and pinkish images, such as those taken with the HDCE-x5 camera. The CMYK color model is most commonly used for printing; it contains M (Magenta) channel, and extends the CMY model by the black (K) color channel. AvgRGB, an averaged grayscale, allows for the analysis of shapes regardless of color differences. In grayscale, pink-colored images taken with the HDCE-x5 camera are more similar to those taken with the Olympus camera, see Fig. 1. STRESS, another grayscale representation, is more sensitive to local changes in lightness. In this representation, contrast is adjusted locally, allowing for better representation of object shapes, and leveling the luminance values of the background in pollen images. It scales the lightness value of each pixel according to two upper and lower envelope functions. These envelope functions are obtained via sampling a number of pixels in the neighborhood (Radius) around the pixel. The algorithm works in several iterations, with sampling only a few pixel values in each iteration. We used STRESS with the following parameters: R(Radius)=1959, M(Number of samples)=10, N(Number of iterations)=100. The radius was adjusted to fit our data, and M and N represent values used in many experiments presented in [13] and recommended therein.

We did not consider the HSL model, as L (Luminance) is calculated as  $L = R * 0.299 + G * 0.587 + B * 0.114$ . Therefore, the Blue channel is almost excluded, whereas Magenta consists of half of the Red and half of the Blue components.

### 3.5 Statistical analysis

We found that the distribution of precision is significantly different from a normal distribution. Therefore, we performed statistical comparisons of the results using a nonparametric test to assess the relative treatment effects (RTE), i.e., the probability that a randomly chosen observation from the whole dataset results in a smaller value than a randomly chosen observation from the studied group. To this end, we applied the F1.LD.F2 design [20], as some of the measures were repeated on the same images. In this design, the test set was used as a grouping variable (2 levels - for 2 sets, see Section 4.1), a model (with 5 levels) was treated as the first sub-plot factor variable, and its repetition (with 3 levels) was treated as the second sub-plot factor variable. ANOVA-type statistic was chosen to test the difference in the precision distribution. Additionally, we compared the precision for different color representations performing multiple comparisons with the Holm-Bonferroni adjustment [11] to control the family-wise error rate.

## 4 Experiments

### 4.1 Datasets

We used two sets of images: the first one taken with Olympus DP 23 microscope camera (available from [14]), and the second one taken with HDCE-x5 microscope camera. The images taken with HDCE-x5 camera show quite uniform

coloration of background, and pollen grains also show similar level of coloration in all images, independent of taxa.

We divided our data into train, validation, and test sets. The train data represented 293 images from the Olympus DP 23 camera. We had 549 objects (pollen grains) for *Alnus*, 312 for *Betula*, and 316 for *Corylus*. The validation data represented 66 images from the Olympus DP 23 camera. We had 143 pollen grains of *Alnus*, 96 *Betula* pollen grains, and 59 grains of *Corylus*.

The test data include:

- **test0**, 38 images taken with Olympus DP 23 camera, containing 72 pollen grains of *Alnus*, 29 grains of *Betula*, and 60 *Corylus* grains, magnified 400x.
- **testH**, 49 images taken with HDCE-x5 camera, containing 14 images for *Alnus* with 41 pollen grains (objects), 20 images for *Betula* with 48 objects, and 15 images for *Corylus* with 42 objects (400x or 600x magnification).

All images represent the same set of biological samples. The data were manually divided into train, validation, and test sets, as some images represented the same area of the investigated sample, but with different focusing. This way we avoided having the same area in train, validation, and test sets. Still, pollen detection and taxon identification can be difficult, as some objects in the images might be out of focus (although the camera focus might be adjusted when taking pictures), overlapping, or only partly visible. If monitoring images were used, other objects (dust, air bubbles) could also be present in these images.

Fig. 1 shows images taken with both Olympus and HDCE-x5 cameras, converted to the representations listed in Section 3.4. The CMYK image looks identical to RGB, but their internal representations differ.

## 4.2 Detectors

We used YOLO12, **small** network architecture with 272 layers and 9254297 parameters, as bigger models applied in similar research gave no improvement [14]. An image size of 640x640 was used as a trade-off between computing speed and quality. We built 5 types of detectors, each one in 3 repetitions (i.e. with different values of random seed):

- 3 models built on original (RGB) images, used as baseline,
- 3 models for CMYK representation,
- 3 models for Magenta channel only, taken from CMY,
- 3 models for grayscale representation using AvgRGB,
- 3 models for grayscale using STRESS with R=1959, M=10, and N=100.

Each detector was trained for 100 epochs, and we chose the model that performed best on the validation dataset. To evaluate these detectors, the test images were converted to the representations mentioned above. The models were tested on both **test0** and **testH**, and the training (and validation) in each case was performed on images in the same representation as the test data. We used a PC with Intel Core i9-14900KS 3.20 GHz, NVIDIA GeForce RTX 4070 Ti SUPER; the training phase for each detector took approximately five minutes, and the average prediction speed was 70 milliseconds per image.

### 4.3 Quality Measures for Model Evaluation

Standard metrics for object detection in images evaluate how well a predicted bounding box aligns with the actual object. Commonly used metrics include mean Average Precision (mAP), specifically mAP@.5 and mAP@[.5:.95]. The mAP@.5 metric assesses accuracy by comparing the predicted bounding box with the ground-truth bounding box using the IoU (Intersection over Union), which quantifies the overlap between two bounding boxes. The bounding box with  $\text{IoU} \geq 0.5$  is considered a hit. The mAP@[.5:.95] metric represents the average mAP calculated across IoU thresholds ranging from 0.5 to 0.95 in increments of 0.05.

Our research differs from standard object detection approaches, as we are less concerned with the exact position of the bounding box. In pollen grain counting, the goal is to achieve classification with 100% precision, i.e., without misclassification of pollen grains. Recall (i.e., omitting grains) is less critical here, as palynologists exclude grains when they are uncertain about the taxon. This is why we selected the precision of the obtained results for statistical analyses.

## 5 Results

Exemplary prediction results are visualized in Fig. 2; we selected two problematic images (with multiple *Betula* pollen grains), captured using two different cameras. We will analyse the results obtained from all three repetitions of each model, but to reduce the number of pictures presented, the best prediction results for each color representation are shown. As we can see, the detection results for the image captured using the HDCE-x5 camera (the bottom row of images) are usually worse than those obtained for the image from the Olympus DP 23 camera (the top row). The only exceptions are the results for the STRESS model. Obviously, it is easier to obtain correct recognition of the taxa when the test image comes from the same dataset as the training data (`test0`). The recognition of pollen grains in the images coming from the `testH` dataset is much more challenging; the detection results are completely wrong for RGB and AvgRGB representations. On the other hand, in the case of STRESS, we get two correct recognitions out of seven grains for the image from `testH` dataset, while we received no correct prediction for the image coming from `test0`. Still, some grains have multiple classes assigned, so they may be counted multiple times, depending on the counting procedure.

Average precision for both test sets, `test0` and `testH`, for 3 repetitions of each detector, is shown in Tab. 1. The results for `test0` are much better than for `testH` for all representations except Magenta. Nonparametric ANOVA shows statistically significant differences in precision between both test sets ( $p\text{-value}=5.19 \cdot 10^{-14}$ ). The results for `test0` are high and stable ( $\text{std} < 4\%$ ), but `testH` shows much greater variability ( $\text{std}$  up to  $\sim 49\%$  for RGB), confirming that the detectors are less reliable when tested on images from a different camera. Only Magenta yields relatively accurate and stable results under these conditions. The detection for RGB is much worse on `testH` than on `test0`, which

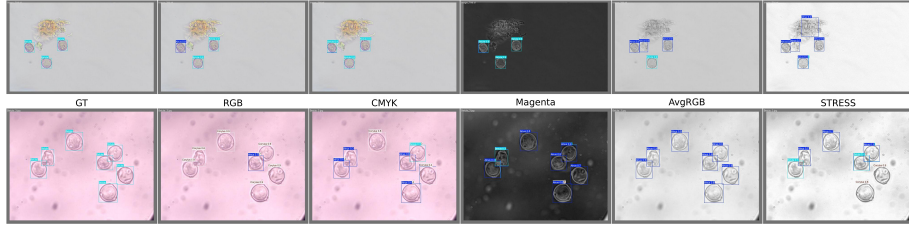


**Fig. 2.** Exemplary predictions obtained for two problematic images taken using HDCE-x5 (the top row) and Olympus DP 23 (the bottom row) microscope cameras. GT stands for ground truth in RGB representation. Images show detections for each color representation. The best results (out of 3 repetitions of each detector) are shown.

shows that the standard RGB representation is not well suited for pollen grain detection.

**Table 1.** Average precision for **test0** and **testH** datasets.

	test0 (mean $\pm$ std) [%]	testH (mean $\pm$ std) [%]
RGB (baseline)	99.62 $\pm$ 1.68	43.69 $\pm$ 48.78
CMYK	99.14 $\pm$ 1.97	76.06 $\pm$ 41.93
Magenta	98.71 $\pm$ 3.63	87.80 $\pm$ 31.27
AvgRGB	99.21 $\pm$ 2.54	67.04 $\pm$ 42.99
STRESS	98.98 $\pm$ 3.39	78.79 $\pm$ 34.30

When both test and train data come from the same camera (**test0**), all results are above 98%, but when the test data come from a different camera (**testH**), precision for particular detectors for each taxon drops dramatically, especially for *Betula* (Fig. 3), except Magenta representation. The precision distribution for each repetition (Fig. 4) shows that this representation is more stable – the outcomes for different repetitions are similar. We conclude that this simple representation, adjusted to the analyzed images, produces very good results.

The nonparametric ANOVA analysis shows the significance of precision differences ( $p\text{-value} < 0.05$ ) for both test sets, and also for other sources of variation (color space, repetition, and all interactions). Therefore, all experimental factors and their interactions significantly influence the precision distribution. Next, we compared the precision results for other color representations with the baseline model (RGB) for **test0** and **testH** separately. The distribution of results for AvgRGB does not differ from the baseline for **test0** (the adjusted  $p\text{-value}$   $p_{adj} = 0.23$ ). In the remaining comparisons, we found significant differences in the precision distribution between the baseline and the other models ( $p_{adj} < 0.05$ ).

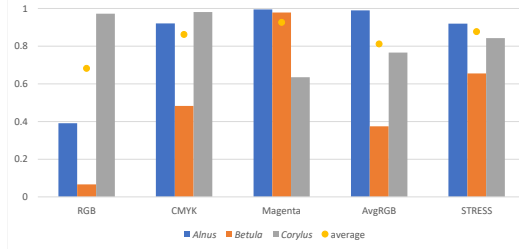


**Fig. 3.** Results for the `testH`. Average precision for each model (marked with a circle) is shown for particular taxa (columns).

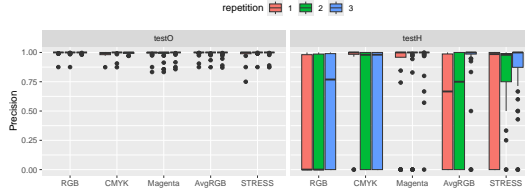


**Fig. 4.** The boxplot showing the precision for 3 repetitions of the detectors for the investigated color representations for images from both test sets.

## 6 Discussion

The results we obtained indicate that adjusting the image representation to the data, in our case stained with fuchsin, significantly improves detection results when the test data are very different from the training data. Comparisons with other studies on pollen grain recognition are challenging because of differences in the datasets used, the number of taxa included, methods of database preparation, and the diverse metrics applied to report results. In [10], automatic localization of pollen grains using video data that captures the focusing process of samples from eleven taxa is investigated, with F1 score of 96% for the localized grains. However, the taxa analyzed and evaluation metrics are different from ours. In [15], 4 taxa were investigated, including taxa investigated here, yielding precision above 90% for YOLO, but test images were taken with the same camera as the training data. Our study is limited to 3 taxa, but they are common allergens in Europe, and their pollen grains are very similar and pose difficulties in automatic detection. We believe that adding other taxa may increase the average precision of trained models.

Our research focuses on light microscopy images. In [23], the identification of pollen grain taxa using various microscopy techniques is investigated, including dark field microscopy and phase contrast microscopy. The results show that the choice of microscopy technique influences recognition quality, supporting our hypothesis that image representation plays a role in the recognition process.

## 7 Conclusion

Our work aimed at automated detection of tree pollen grains, representing three allergenic taxa, namely *Betula*, *Corylus*, and *Alnus*, in microscopy images. The analyzed slides are colored with fuchsin, thus pollen grains are pinkish in these images. Additionally, a camera may also introduce pinkish shade to the image. We investigated whether changing image representation could enhance detection quality, particularly for images from different cameras or with varying color saturation. We found that the models trained on a particular image set may learn image features typical of a camera, and not of particular taxa. Our analyses allow us to conclude that image representation, as well as the camera applied for data acquisition, can significantly change the quality of object detection in images. In our experiments, Magenta works best, as the precision results are relatively high and stable. Therefore, even if the representation is simpler than the original one (with one instead of three image components), but adjusted to the coloration of images, better detection could be obtained.

The taxa used in our study produce pollen grains of similar structural features. Pollen grains of other plants may also be found in slides from pollen monitoring, together with the analyzed taxa, but they have different structural features and they would be easier to distinguish by detectors.

As a future work, we would like to collect more data, apply other detectors (DETR), and use the investigated simple single-channel representations that yielded best detection results for pollen images, mainly Magenta. Additionally, some of our images include out-of-focus pollen grains and have various brightness levels. This may deteriorate the results, so we are going to investigate how changes in the light levels influence the quality of pollen grain detection.

## References

1. Ultralytics YOLO Docs (2025), <https://docs.ultralytics.com/models/>
2. Ascani, L., Novara, C., Dusio, V., Oddi, L., Siniscalco, C.: Quantitative methods in microscopy to assess pollen viability in different plant taxa. *Plant Reprod.* **33**, 205–219 (2020)
3. Astolfi, G., Gonçalves, A., Menezes, G., Borges, F., Astolfi, A., Matsubara, E., Alvarez, M., Pistori, H.: POLLEN73S: An image dataset for pollen grains classification. *Ecological Informatics* **60** (2020)
4. Bell, K., Burgess, K., Botsch, J., Dobbs, E., Read, T., Brosi, B.: Quantitative and qualitative assessment of pollen DNA metabarcoding using constructed species mixtures. *Molecular Ecology* **28**, 431–455 (2019)
5. Cao, N., Meyer, M., Thiele, L., Saukh, O.: Automated pollen detection with an affordable technology. In: EWSN. p. 108–119 (2020)
6. Carion, N., Massa, F., Synnaeve, G., Usunier, N., Kirillov, A., Zagoruyko, S.: End-to-end object detection with transformers (2020), <https://arxiv.org/abs/2005.12872>
7. Chen, K., Chen, X., Sui, G.: Pollen detection through integrated microfluidics and smartphone-driven deep learning systems. *Results Eng.* **24**, 102867 (2024)

8. Dunker, S., Motivans, E., Rakosy, D., Boho, D., Mäder, P., Hornick, T., Knight, T.: Pollen analysis using multispectral imaging flow cytometry and deep learning. *New Phytologist* **229**(1), 593–606 (2021)
9. France, I., Duller, A., Duller, G., Lamb, H.: A new approach to automated pollen analysis. *Quaternary Science Reviews* **19**(6), 537–546 (2000)
10. Gallardo, R., García-Orellana, C., González-Velasco, H., García-Manso, A., Tormo-Molina, R., Macías-Macías, M., Abengózar, E.: Automated multifocus pollen detection using deep learning. *Multimed. Tools Appl.* **83**, 72097–72112 (2024)
11. Giacalone, M., Agata, Z., Cozzuoli, P.C., Alibrandi, A.: Bonferroni-Holm and permutation tests to compare health data: methodological and applicative issues. *BMC Medical Research Methodology* (2018)
12. Hirst, J.M.: An automatic volumetric spore trap. *Annals of Applied Biology* **39**, 257–265 (1952). <https://doi.org/10.1111/j.1744-7348.1952.tb00904.x>
13. Kolås, Ø., Farup, I., Rizzi, A.: STRESS: A framework for spatial color algorithms. *Journal of Imaging Science and Technology* **55**, 040503 (01 2011)
14. Kubera, E., Kubik-Komar, A., Kurasinski, P., Piotrowska-Weryszko, K., Skrzypiec, M.: Detection and recognition of pollen grains in multilabel microscopic images. *Sensors* **22**(7) (2022). <https://doi.org/10.3390/s22072690>
15. Kubera, E., Kubik-Komar, A., Wieczorkowska, A., Piotrowska-Weryszko, K., Kurasinski, P., Konarska, A.: Towards automation of pollen monitoring: Image-based tree pollen recognition. In: ISMIS, LNCS, vol. 13515, pp. 219–229. Springer (2022)
16. Lin, T.Y., Maire, M., Belongie, S., Bourdev, L., Girshick, R., Hays, J., Perona, P., Ramanan, D., Zitnick, C.L., Dollár, P.: COCO - common objects in context (2014), <https://arxiv.org/abs/1405.0312>
17. Martin, A., Harvey, W.: The global pollen project: a new tool for pollen identification and the dissemination of physical reference collections. *Methods in Ecology and Evolution* **8**(7), 892–897 (2017)
18. McDevitt, S., Rosselot, G.: Highly allergic travelers. CDC yellow book 2024 (2024), <https://wwwnc.cdc.gov/travel/page/yellowbook-home>
19. Meersens: Pollen allergy cost (2025), <https://meersens.com/pollen-allergy-cost-how-pollen-data-revolutionize-healthcare-systems/?lang=en>
20. Noguchi, K., Gel, Y.R., Brunner, E., Konietzschke, F.: nparLD: An R software package for the nonparametric analysis of longitudinal data in factorial experiments. *Journal of Statistical Software* **50**(12), 1–23 (2012)
21. Olsson, O., Karlsson, M., Persson, A., Smith, H., Varadarajan, V., Yourstone, J., Stjernman, M.: Efficient, automated and robust pollen analysis using deep learning. *Methods in Ecology and Evolution* **12**, 850–862 (2021)
22. Plaza, M., Kolek, F., Leier-Wirtz, V., Brunner, J., Traidl-Hoffmann, C., Damialis, A.: Detecting airborne pollen using an automatic, real-time monitoring system: Evidence from two sites. *Int J Environ Res Public Health* **19**(4) (2022)
23. Pospiech, M., Javůrková, Z., Hrabec, P., Štarha, P., Ljasovská, S., Bednář, J., Tremlová, B.: Identification of pollen taxa by different microscopy techniques. *PLoS One* **16**(9) (2021)
24. Redmon, J., Divvala, S., Girshick, R., Farhadi, A.: You only look once: Unified, real-time object detection. In: CVPR. pp. 779–788. IEEE, Las Vegas, USA (2016)
25. Ren, S., He, K., Girshick, R., Sun, J.: Faster R-CNN: Towards real-time object detection with region proposal networks. In: NeurIPS, vol. 28 (2015)
26. Sevillano, V., Holt, K., Aznarte, J.: Precise automatic classification of 46 different pollen types with convolutional neural networks. *PLoS ONE* **15** (2020)